Available on CMS information server

CMS NOTE 2006/133

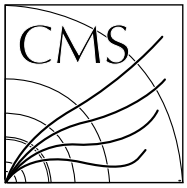

The Compact Muon Solenoid Experiment

CMS Note

Mailing address: CMS CERN, CH-1211 GENEVA 23, Switzerland

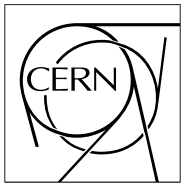

21 April 2006

Leptons + Jets + Missing Energy analysis at LM1

M. Chiorboli, M. Galanti, A. Tricomi

University of Catania and INFN Catania, Italy

Abstract

The Leptons + Jets + Missing Energy (l = e,μ) final state for SUSY events is investigated at mSUGRA benchmark point LM1. The end point in the dilepton pair invariant mass distribution is reconstructed and a scan of the $(m_0,\, m_{1/2})$ plane is performed in order to determine the observability reach.

1 Introduction

If SUSY exists at the electroweak scale, it will be probably first detected using inclusive signatures. However, if new particles are observed, it is necessary to measure, in a second stage, their masses and their couplings. Eventually, with a deep knowledge of the spectrum of the observed particles, it could be desirable to extrapolate the model parameters from the measured quantities.

In a R-parity conserving scenario the decay products of a SUSY particle always include an invisible $\tilde{\chi}_1^0$, therefore no exclusive mass peak can be reconstructed directly. Many SUSY decay chains, however, show a sequential decay structure which can be exploited to determine combinations of masses by measuring the end points of the visible mass distribution [1]. The value of each end point is in fact related to the masses of SUSY particles involved and a measurement of enough end points gives a fully constrained system of equations, which can be solved in order to extract the masses. Moreover, the end points depend only on the kinematic features of the decays, making this method largely independent from the SUSY model employed. The SUSY production cross section at LHC is dominated by gluinos and squarks which decay mainly through a chain to the lightest neutralinos. For low and moderate $\tan\beta$ values, many decay chains end up with the decays of the second neutralino. Particularly interesting are the decays $\tilde{\chi}_2^0 \rightarrow \tilde{\chi}_1^0 l^+ l^-$ and $\tilde{\chi}_2^0 \rightarrow \tilde{l}_R l \rightarrow \tilde{\chi}_1^0 l^+ l^-$, with $l = e, \mu$, in which the two final state leptons provide a natural trigger. Leptons (electrons and muons) from the $\tilde{\chi}_2^0$ decay exhibit a peculiar l^+l^- invariant mass distribution with a sharp edge. If $m_{\tilde{\chi}_2^0} < m_{\tilde{l}} + m_{ll}$ the $\tilde{\chi}_2^0$ decay would be a three body decay mediated by a virtual slepton and the edge would be placed at $m_{\tilde{\chi}_2^0} - m_{\tilde{\chi}_1^0}$. Conversely, when $m_{\tilde{\chi}_2^0} > m_{\tilde{l}} + m_{ll}$, the neutralino decay is a two body decay and the edge would be placed at $M_{l^+l^-}^{max} = \sqrt{\left(m_{\tilde{\chi}_2^0}^2 - m_{\tilde{l}}^2\right)\left(m_{\tilde{l}}^2 - m_{\tilde{\chi}_1^0}^2\right)}/m_{\tilde{l}}$. Which of the two body or three body decay is kinematically allowed depends on the parameter space, however for moderate $\tan\beta$ at least one of these decay modes is generally available.
In order to reconstruct sparticle masses, it is hence fundamental to start the reconstruction with the $\tilde{\chi}_2^0 \rightarrow \tilde{l}^{\pm} l^{\mp} \rightarrow \tilde{\chi}_1^0 l^+ l^-$ decay chain. In this note the method to reconstruct the dilepton end point is described. We proved the feasibility of the method at benchmark point LM1 ($\mathrm{m_0} = 60\ \mathrm{GeV}/c^2$, $\mathrm{m_{1/2}} = 250\ \mathrm{GeV}/c^2$, $\mathrm{A_0} = 0$, $\tan\beta = 10$, $\mathrm{sgn}(\mu) = +1$) [2]. Moreover, we studied the statistical significance of the dilepton+jets+missing transverse energy channel in the mSUGRA (m_0, $m_{1/2}$) plane for $\tan\beta = 10$ and for integrated luminosities of 1, 10 and 30 fb^{-1}.

In order to reconstruct the decay chain $\tilde{\chi}_2^0 \rightarrow \tilde{l}^{\pm} l^{\mp} \rightarrow \tilde{\chi}_1^0 l^+ l^-$, final states with at least two same-flavour opposite-sign (SFOS) leptons are selected. In this note, leptons indicate electrons and muons, and no taus are considered in the final state. Since this decay chain is the last step of a longer one coming from the decays of squarks and/or gluinos, signal events are also characterised by the presence of jets and missing transverse energy. Hence, in this note final states with dileptons+jets+missing transverse energy are considered.

2 Signal

The LM1 mSUGRA benchmark point has been chosen as the working point. At point LM1 the total NLO production cross section of supersymmetric events, calculated with PROSPINO [3], is ~ 52 pb, dominated by $\tilde{q}\tilde{g}$, $\tilde{g}\tilde{g}$ and $\tilde{q}\tilde{\bar{q}}$ processes. The mSUGRA parameters at LM1 and the main branching ratios relevant for this analysis are shown in Table 1.

Table 1: mSUGRA parameters and main branching ratios at benchmark point LM1.

$M_{1/2}$	250 GeV/c^2
M_0	60 GeV/c^2
sign(μ)	+
A_0	0
tan(β)	10
$M_{\tilde{\chi}_2^0}$	179.6 GeV/c^2
$M_{\tilde{\ell}_R}$	118.88 GeV/c^2
$M_{\tilde{\chi}_1^0}$	94.92 GeV/c^2
M_{ll}^{max}	81.04 GeV/c^2
BR$\left(\tilde{\chi}_2^0 \rightarrow \tilde{\ell}^{\pm}\ell^{\mp} \rightarrow \tilde{\chi}_1^0 \ell^{\pm}\ell^{\mp}\right)$	11.2%
BR$\left(\tilde{\chi}_2^0 \rightarrow \tilde{\chi}_1^0 \ell^{\pm}\ell^{\mp}\right)$	negligible
Inclusive cross section	52 pb

Table 2: L1 trigger bits with $\varepsilon_1 > 60\%$ for SUSY events.

Bit #	Trigger condition	Threshold (low lumi)	ε_1	ε_2
0	Single muon	$P^T > 14$ GeV/c	22.0%	58.5%
1	Di-muon	$P^T > 3$ GeV/c	11.5%	53.3%
2	Single isolated e/γ	$E^T > 23$ GeV (29 GeV @ 95% eff)	71.7%	91.3%
3	Isolated di-e or di-γ	$E^T > 12$ GeV (17 GeV @ 95% eff)	38.6%	71.6%
4	Di-e or di-γ	$E^T > 19$ GeV	44.0%	72.1%
7	Missing transverse energy	$E^T > 140$ GeV	65.7%	84.6%
20	1 μ + 1 central jet	$P^T > 5$ GeV/c, $E^T > 30$ GeV	30.9%	61.7%
22	1 μ + 1 τ jet	$P^T > 5$ GeV/c, $E^T > 25$ GeV	25.5%	50.8%
23	1 μ + missing energy	$P^T > 5$ GeV/c, $E^T > 45$ GeV	32.2%	65.0%
24	1 isolated e/γ + 1 central jet	$E^T > 21$ GeV, $E^T > 45$ GeV	65.9%	84.6%
26	1 isolated e/γ + 1 τ jet	$E^T > 14$ GeV, $E^T > 52$ GeV	43.0%	70.6%
27	1 isolated e/γ + missing energy	$E^T > 21$ GeV, $E^T > 75$ GeV	65.8%	89.7%
28	1 central jet + missing energy	$E^T > 88$ GeV, $E^T > 46$ GeV	76.8%	84.4%
30	1 tau jet + missing energy	$E^T > 35$ GeV, $E^T > 40$ GeV	61.0%	81.4%

The invariant mass distribution of leptons coming from the $\tilde{\chi}_2^0$ at parton level is also shown in Fig. 1.

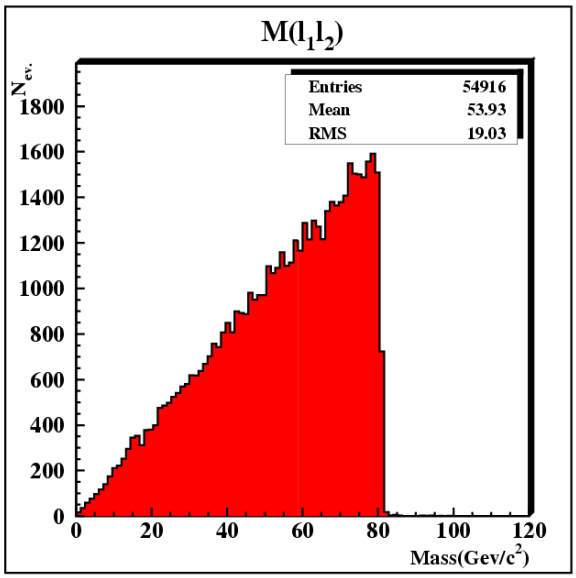

Figure 1: Dilepton invariant mass distribution at generator level.

2.1 Event Generation and Simulation

The events analysed in this note have been produced using PYTHIA 6.225 [4] interfaced with ISAJET 7.69 [5]. A full detector simulation has been employed, using OSCAR 3.6.5 [6], and reconstruction has been performed through ORCA 8.7.4 [7]. Low luminosity pile-up has also been taken into account.

2.2 Trigger

The L1 trigger bits with highest efficiency for signal, numbered according to the official ORCAnumbering scheme, are shown in Table 2. In the table, ε_1 gives the total trigger efficiency for that trigger bit, that is the ratio between the number of events in which the trigger bit is true, and the total number of simulated events. The second value in Table 2, ε_2, is the trigger efficiency after cuts, that is the number of events selected by analysis cuts for which a trigger bit is activated, divided by the total number of events passing analysis cuts.

The HLT trigger bits with highest efficiency for SUSY events are shown in Table 3. The two efficiencies shown are defined in a similar way as for the L1 case. Although electron triggers have the highest efficiency, they don't seem

Table 3: Main HLT trigger bits for SUSY events.

Bit #	Trigger name	ε_1	ε_2
0	L2 electron trigger	70.9%	88.6%
1	L25 electron trigger	60.0%	81.5%
2	HLT electron trigger	12.4%	46.2%
6	Double electron trigger	21.9%	56.9%
17	L2 photon trigger	71.0%	88.6%
36	L2 muon trigger	17.5%	55.9%
39	HLT muon trigger	10.1%	48.5%
54	Double muon trigger	2.6%	41.9%
65, 72	L2 pixel tau trigger: P^T cut	89.1%	96.1%
70	L2 pixel tau trigger: isolation	87.2%	96.0%
75, 82	L2 tracker tau trigger: P^T cut	89.1%	96.1%
76, 80,83	L2 tracker tau trigger: isolation	89.1%	96.1%
116	L2 MET trigger for tau	89.4%	99.2%
117	L2 tau trigger: P^T cut	84.8%	93.0%
118	L2 tau trigger: isolation	84.8%	93.0%
124	Single jet trigger	80.6%	91.9%
128	MET trigger	82.6%	98.2%
134, 140	Single jet for b trigger	77.6%	85.9%

Table 4: Efficiencies for the five trigger streams applied to the SUSY events

Stream	L1	HLT	ε	N_{ev} in 1 fb^{-1}
JetMET	76.8%	66.0%	1.44%	751
Single Lepton	78.5%	21.4%	1.64%	853
LeptonMet	75.5%	17.6%	1.61%	835
LeptonJet	74.2%	16.4%	1.38%	719
Dilepton	50.5%	23.4%	1.50%	828

to be activated by real electrons only, but also by jets faking electrons. In fact, the corresponding muon triggers have a lower efficiency, even though muons and electrons produced in LM1 SUSY events have roughly the same kinematical features.

In order to choose the best possible trigger stream for the topology under investigation, five different streams have been compared. They are defined as follows:

- JetMET: L1 bit 28 (JetMET), HLT bit 124 and 128 (single jet and MET);
- Single Lepton: L1 bit 0 or 2 (single muon or single e/γ), HLT bit 2 or 39 (HLTelectrons or HLT muons);
- LeptonMET: L1 bit 23 or 27 (1 muon + MET or 1 e/γ + MET), HLT bit 2 or 39 and 128 (HLTelectrons or HLTmuons and MET);
- LeptonJet: L1 bit 20 or 24 (1 muon + Jet or 1 e/γ + Jet), HLT bit 2 or 39 and 124 (HLTelectrons or HLTmuons and Jet);
- Dilepton: L1 bit 1 or 4 (di-muon or di-e/γ), HLT bit 6 or 54 (doubleElectron or doubleMuon);

Table 4 shows the L1 and HLT efficiencies for the five streams, before any selection cut. The column indicated with ε shows the efficiency after all the selection cuts which will be described in the next sections. Before any selection cut is applied, the JetMET stream has the largest efficiency: this can be understood considering the presence of the neutralinos in all the SUSY events and the high jet multiplicity in most of the events. After the selection cuts the Single Lepton trigger gives the best efficiency, since the cuts are optimized to look at the presence of leptons in the final state. The Single Lepton trigger is hence the stream chosen for this analysis.

2.3 Electrons

Among all recontructed electrons, only the isolated ones are looked for. Therefore, a cleaning of the electron sample is required, since the standard CMS reconstruction algorithm also yields a great number of fakes, that can

be either non-isolated electrons coming from jets, or misidentified jets. Reconstructed electrons are required to have $P^T > 10$ GeV/c. In addition, the ΔR ($R = \sqrt{\eta^2 + \varphi^2}$) between any two electrons must be larger than 0.2, in order to exclude a large number of fake dilepton couples with low invariant mass.

An isolation criterion is applied in the tracker, by rejecting electrons if the ΣP^T of the tracks within $\Delta R = 0.25$ around the electron is larger than 5 GeV/c.

In order to reject the fakes, the EleID tool was used [9], which assigns to each reconstructed electron a likelihood, taking values between 0 and 1. Variables used for the likelihood calculation are:

- E/p
- $\sigma_{\eta\eta} = \Sigma_{5\times5} \left(\eta_{crystal} - \eta_{seed}\right)^2 \mathrm{E}_{crystal}/\mathrm{E}_{5\times5}$
- $\Delta\eta = |\eta_{supercluster} - \eta_{track}|$
- H/E
- $\mathrm{E}_{3\times3}/\mathrm{E}_{5\times5}$.

The likelihood for all reconstructed electrons in LM1 events is shown in Fig. 2. A cut of 0.65 in the likelihood has been chosen.

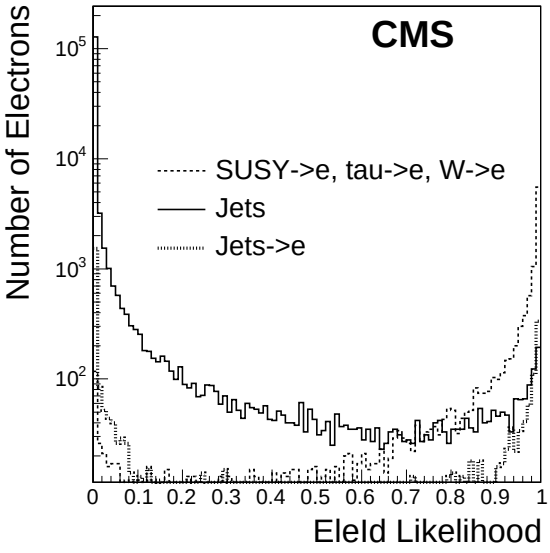

Figure 2: Electron likelihood for the signal sample.

The distributions of the 5 EleID variables for the signal events, for fake and real electrons separately, are shown in Figures 3 and 4. Before the selection, distributions are quite different, whereas after the selection, only fake electrons with features similar to the true ones survive. The working point chosen corresponds to a selection efficiency of about 91%, with a purity of 79%, as shown in Figure 5.

2.4 Muons

Muon selection has been performed through a cut-based approach. Each muon is required to have $P^T > 10\,\mathrm{GeV}/c$, and $\Delta R > 0.15$ from another muon. The same isolation criterion as for electrons is also applied.

If more than two opposite sign muons or electrons survive cuts, all possible l^+l^- combinations that can be formed out of them are used for the analysis.

The invariant mass distributions of same flavour opposite sign electron (Fig. 6) and muon (Fig. 7) pairs for signal only after trigger and lepton selection show that the characteristic edge behaviour is well visible with an integrated luminosity of 1 fb^{-1}.

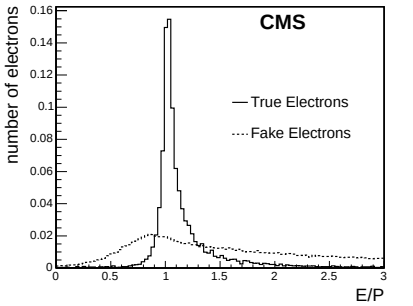

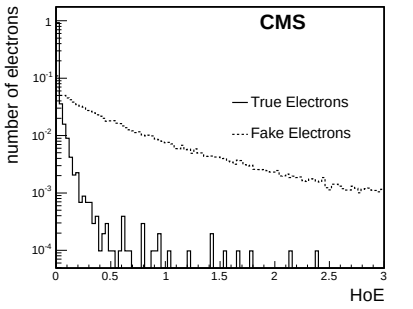

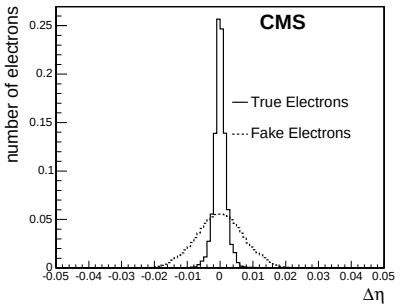

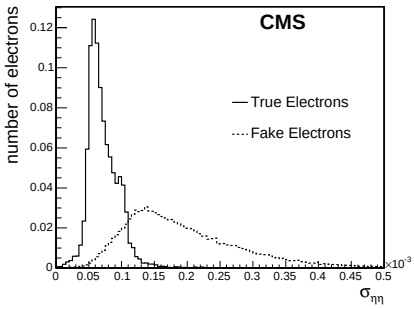

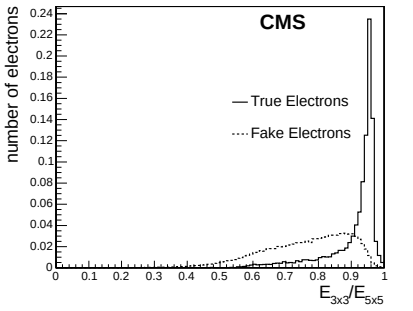

Figure 3: From top to bottom: distributions of E/p, H/E, $\Delta\eta$, $\sigma_{\eta\eta}$, and $E_{3\times3}/E_{5\times5}$ before the likelihood cut.

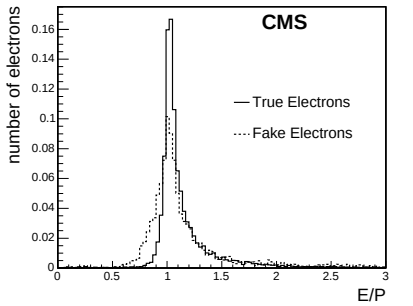

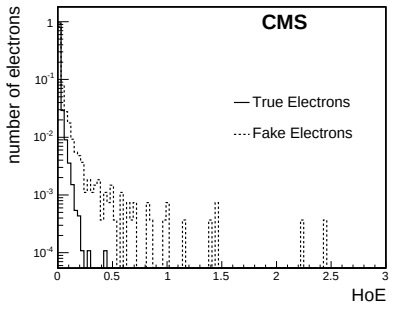

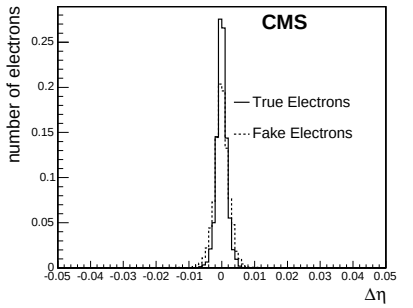

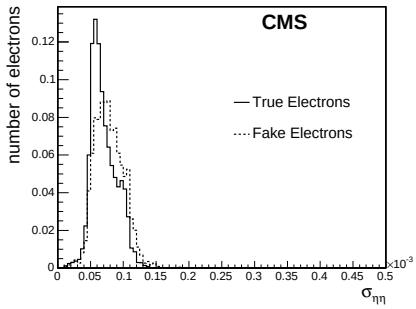

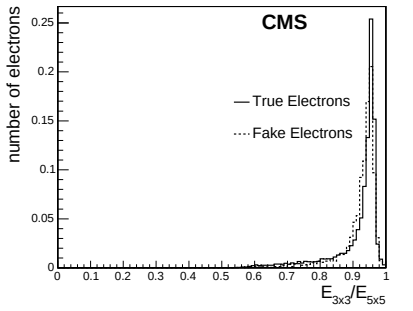

Figure 4: Distributions after the likelihood cut.

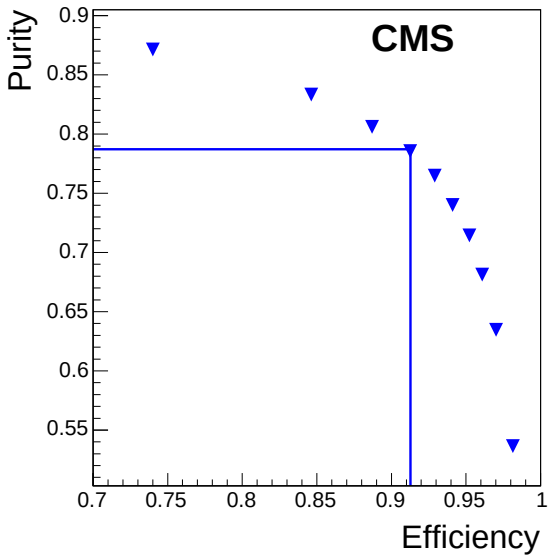

Figure 5: Efficiency vs. purity for different values of EleID cut. The working point with Likelihood> 0.65 is indicated.

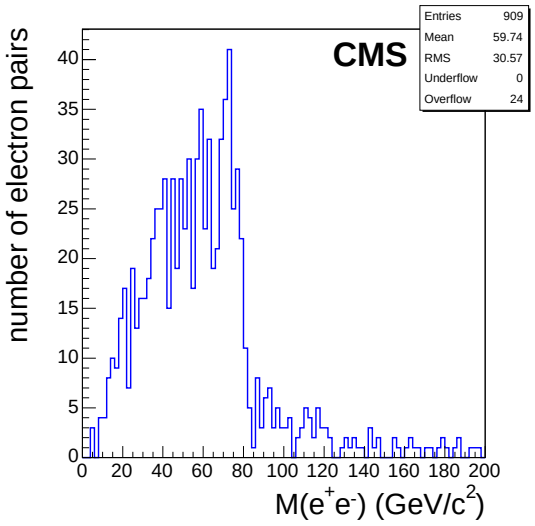

Figure 6: Opposite sign electron pair invariant mass distribution after trigger and lepton selection for 1 fb^{-1}.

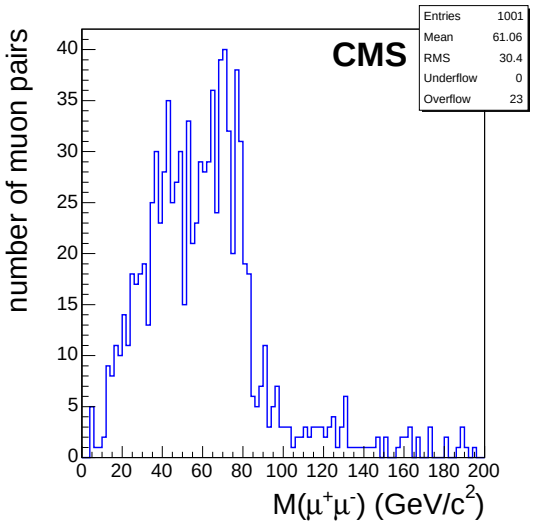

Figure 7: Opposite sign muon pair invariant mass distribution after trigger and lepton selection for 1 fb^{-1}.

3 Background

The Standard Model backgrounds considered for this analysis are: $\mathrm{t\bar{t}}$, WW+jets, DY $\rightarrow 2l$, Zbb $\rightarrow llbb$, W+jets, Z+jets, QCD, ZZ+jets and $\mathrm{t\bar{t}b\bar{b}}$. All background events are taken from the official CMS production. They have been generated with PYTHIA. The Zbb background only has been generated using PYTHIAinterfaced with COMPHEP [10]. The full simulation of the detector has been used also for the backgrounds. In order to suppress Standard Model background the full topology of the SUSY events is exploited. Thus, additional cuts on jets and missing transverse energy are applied.

3.1 Jets

Jets are reconstructed through the iterative cone algorithm with the gamma jet correction [11], with a cone of $\Delta R = 0.5$. The P^Tdistributions of the leading and of the second leading jet respectively for signal and for $\mathrm{t\bar{t}}$ events are shown in Figures 8 and 9. In this analysis at least 2 jets are required with $P^T_{jet1} > 100$ GeV/c, $P^T_{jet2} > 60$ GeV/c.

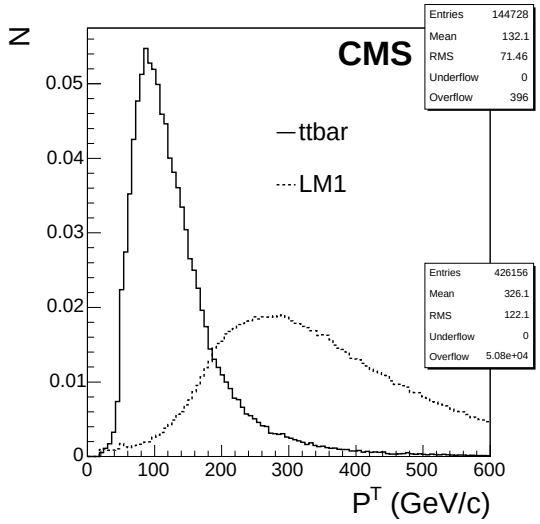

Figure 8: P^Tdistribution of the leading jet for SUSY and $\mathrm{t\bar{t}}$ events.

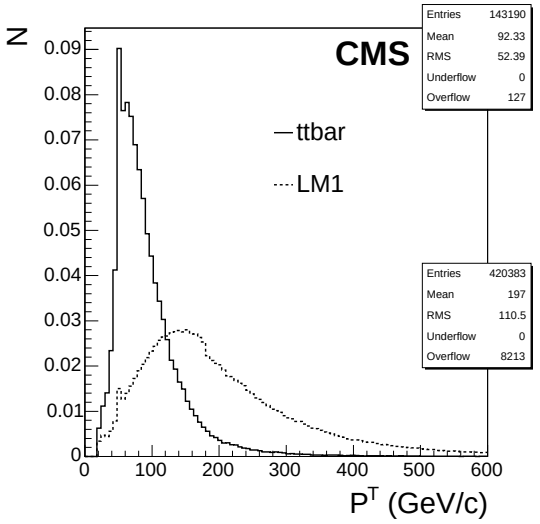

Figure 9: P^Tdistribution of the second leading jet for SUSY and $\mathrm{t\bar{t}}$ events.

3.2 Missing transverse energy

In order to measure the missing transverse energy (MET) of an event, two algorithms were tried. The first algorithm was based on the information from the hadronic and electromagnetic calorimeters as treated in ORCA [12], while the second one was a custom algorithm, described below.

In the custom algorithm the MET calculation is done by summing up all the energies of isolated muons, isolated and EleID selected electrons, and jets. In order to avoid double counting of leptons, electrons are removed from the MET calculation if their ΔR with respect to a muon is less than 0.002. Similarly, jets are excluded from the sum if they are close to electrons. In addition, jets are counted in the calculation of the MET only if they have $P^T > 30$ GeV/c.

This quantity is usually called Missing HT: it is equivalent to the standard MET calculated setting very high thresholds on the calorimeter cells, which is known to produce large resolution tails depending on the fluctuations between the high P^T and low P^T sharing of energy. In the rest of the paper we keep the name MET to indicate the Missing HT.

An event passes the MET cut if it has a missing $E^T > 200$ GeV (Fig. 10). Although this custom MET has the advantage of giving a higher selection efficiency for signal events, and a higher background rejection, especially for $\mathrm{t\bar{t}}$ events, with respect to the standard MET, the modeling of the custom MET is heavily dependent on the underlying event and pileup modeling and is subject to larger systematic errors.

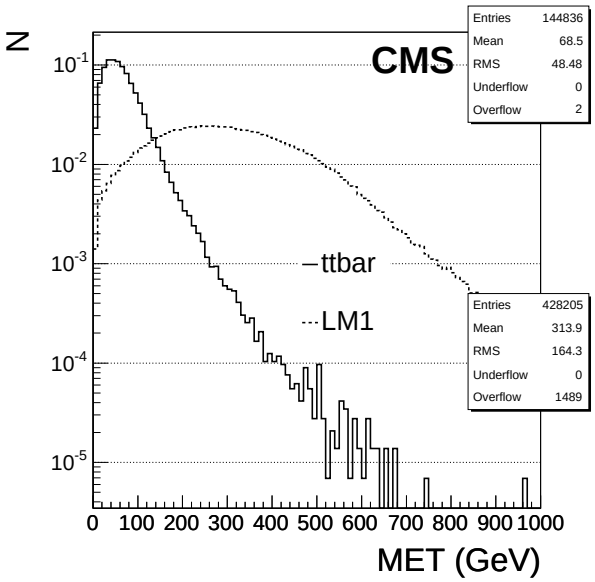

Figure 10: Distribution of the custom missing transverse energy for SUSY and $\mathrm{t\bar{t}}$ events.

3.3 Background rejection

Table 5 summarizes the number of expected events in 1 fb^{-1} for SUSY events and the Standard Model backgrounds considered, after all the selections applied:

- at least two same-flavour opposite-sign isolated leptons, with $P^T > 10$ GeV/c and $|\eta| < 2.4$ for both electrons and muons;
- at least two jets with $P^T_{j1} > 100$ GeV/c and $P^T_{j2} > 60$ GeV/c and $|\eta| < 3.0$;
- $E^T_{miss} > 200$ GeV.

The background processes with the highest cross section are Drell-Yan and Z(W)+jets, but after selection cuts only few events survive. The $\hat{P}^T$ bins of the Z(W)+jets processes for which no events are selected in the samples used are not shown in the table. Suppression is less effective for inclusive $\mathrm{t\bar{t}}$, which ends up being the main source of background events after cuts, with 155 events passing them for 1 fb^{-1} of integrated luminosity. The second background source in order of importance is WW+jets, since 26 events are expected to survive cuts for 1 fb^{-1}. The Z+jets background gives a contribution of about 24 events. All the other backgrounds considered are effectively suppressed by the cuts applied. The QCD background is not shown in the table. No events have been selected out of the 668 thousands QCD events used, divided in 14 different $\hat{P}^T$ bins. Requiring only the presence of two SFOS isolated leptons, without applying trigger requirements, the MET selection or the Jet selection, only one event is selected in the bin 600 GeV/$c < \hat{P}^T <$ 800 GeV/c, in which the cross section in only four times larger than the SUSY LM1 one. In order to be confident of the negligible contribution from the QCD events, the MET and lepton selections have been applied one-by-one. The product of the corresponding efficiencies gives a very low expected number of events at 1 fb^{-1} (Table 6). The trigger selection and the jet requirement have not been considered in this calculation, since they are strongly correlated to the lepton and MET selection, respectively. An extrapolation of the possible contribution of the QCD background on this analysis has also been tried, considering a similar analysis by CDF [13], in which the contribution from $\mathrm{b\bar{b}}$ and $\mathrm{c\bar{c}}$ is estimated to be about 0.25 times the contribution from $\mathrm{t\bar{t}}$. Considering the same ratio for this analysis, the number of QCD events selected in 1 fb^{-1} should be about 1/4 of the number of selected $\mathrm{t\bar{t}}$, that is 155/4 = 38.8. This number is overestimated due to the larger increase of the $\mathrm{t\bar{t}}$ cross section from TeVatron to LHC energy with respect to the corresponding increase of the $\mathrm{b\bar{b}}$ and $\mathrm{c\bar{c}}$ cross sections. The method of the factorization of the efficiencies has been used also for the low $\hat{P}^T$ bins of the Z(W)+jets processes, giving similar results: an upper limit of the order of the single event is given in each bin.

The total number of SUSY events after all selection cuts is 853 in 1 fb^{-1}, corresponding to an efficiency of 1.6% over the whole SUSY sample.

Table 5: Selection efficiencies and number of events surviving cuts for signal and background processes. For the W+jets and Z+jets samples, only the $\hat{P}^T$ bins in which at least one event is selected are shown.

Process	σ (pb)	Ev. analysed	ε_{MEAS}	N_{ev} in 1 fb^{-1}
SUSY (LM1)	52	478k	0.016	853
$t\bar{t}$	830	913k	$1.9{\cdot}10^{-4}$	155
WW+jets	188	197k	$1.4{\cdot}10^{-4}$	26
DY$\rightarrow 2\mu$	$3.97{\cdot}10^{3}$	916k	$< 1.1{\cdot}10^{-6}$	< 4
DY$\rightarrow 2\tau$	$3.97{\cdot}10^{3}$	514k	$1.9{\cdot}10^{-6}$	7.7
Zbb$\rightarrow$eebb $60 < \hat{P}^T < 100$ GeV/c	26	73k	$1.5{\cdot}10^{-4}$	3.9
Zbb$\rightarrow$eebb $\hat{P}^T > 100$ GeV/c	1	187k	$1.6{\cdot}10^{-4}$	0.2
Zbb$\rightarrow \mu\mu$bb $60 < \hat{P}^T < 100$ GeV/c	26	41k	$1.1{\cdot}10^{-5}$	0.3
Zbb$\rightarrow \mu\mu$bb $\hat{P}^T > 100$ GeV/c	1	88k	$9.8{\cdot}10^{-5}$	0.1
Zbb$\rightarrow \tau\tau$bb $60 < \hat{P}^T < 100$ GeV/c	3.3	60k	$7.8{\cdot}10^{-5}$	0.3
Zbb$\rightarrow \tau\tau$bb $\hat{P}^T > 100$ GeV/c	0.13	180k	$1.8{\cdot}10^{-4}$	0.03
W+jets $400 < \hat{P}^T <$700 GeV/c	48.8	41k	$2.4 \cdot 10^{-5}$	1.2
W+jets $700 < \hat{P}^T <$1100 GeV/c	4.9	24k	$8.3 \cdot 10^{-5}$	0.4
Z+jets $50 < \hat{P}^T <$85 GeV/c	983.7	237k	$4.2 \cdot 10^{-6}$	4.2
Z+jets $85 < \hat{P}^T <$150 GeV/c	304.8	243k	$1.6 \cdot 10^{-5}$	5
Z+jets $150 < \hat{P}^T <$250 GeV/c	69	34k	$1.7 \cdot 10^{-4}$	12.2
Z+jets $250 < \hat{P}^T <$400 GeV/c	3.7	12k	$2.5 \cdot 10^{-4}$	0.9
ZZ+jets	11	37k	$2.6{\cdot}10^{-4}$	2.9
$t\bar{t}b\bar{b}$	3.3	50k	$9.8{\cdot}10^{-4}$	3.2

Table 6: Factorized efficiencies for QCD events.

$\hat{P}^T$ bin	σ (pb)	Ev. analysed	ε_{MET}	ε_{2lep}	ε_{TOT}	N_{ev} in 1 fb^{-1}
50-80	$2.09{\cdot}10^{7}$	47k	$< 2.1{\cdot}10^{-5}$	$< 2.1{\cdot}10^{-5}$	$< 4.4{\cdot}10^{-10}$	< 9.2
80-120	$2.95{\cdot}10^{6}$	48k	$2.1{\cdot}10^{-5}$	$< 2.1{\cdot}10^{-5}$	$< 4.4{\cdot}10^{-10}$	< 1.3
120-170	$4.00{\cdot}10^{5}$	49k	$< 2.0{\cdot}10^{-5}$	$< 2.0{\cdot}10^{-5}$	$< 4.0{\cdot}10^{-10}$	$< 1.6{\cdot}10^{-1}$
170-230	$1.01{\cdot}10^{5}$	47k	$8.5{\cdot}10^{-5}$	$< 2.1{\cdot}10^{-5}$	$< 1.8{\cdot}10^{-9}$	$< 1.8{\cdot}10^{-1}$
230-300	$2.39{\cdot}10^{4}$	34k	$6.8{\cdot}10^{-4}$	$< 2.8{\cdot}10^{-5}$	$< 1.9{\cdot}10^{-8}$	$< 4.6{\cdot}10^{-1}$
300-380	$6.39{\cdot}10^{3}$	66k	$2.8{\cdot}10^{-3}$	$< 1.5{\cdot}10^{-5}$	$< 4.2{\cdot}10^{-8}$	$< 2.7{\cdot}10^{-1}$
380-470	$1.89{\cdot}10^{3}$	67k	$7.8{\cdot}10^{-3}$	$< 1.5{\cdot}10^{-5}$	$< 1.2{\cdot}10^{-7}$	$< 2.2{\cdot}10^{-1}$
470-600	$6.90{\cdot}10^{2}$	62k	$1.7{\cdot}10^{-2}$	$< 1.6{\cdot}10^{-5}$	$< 2.7{\cdot}10^{-7}$	$< 1.9{\cdot}10^{-1}$
600-800	$2.02{\cdot}10^{2}$	56k	$3.5{\cdot}10^{-2}$	$1.8{\cdot}10^{-5}$	$6.3{\cdot}10^{-7}$	$1.3{\cdot}10^{-1}$
800-1000	$3.57{\cdot}10^{1}$	23k	$6.9{\cdot}10^{-2}$	$< 4.3{\cdot}10^{-5}$	$< 3.0{\cdot}10^{-6}$	$< 1.1{\cdot}10^{-1}$

4 Results at LM1

The invariant mass distribution of the same flavour opposite sign lepton pairs after all selection cuts and for an integrated luminosity of 1 fb^{-1} is shown, superimposed over the $t\bar{t}$ background, in Figure 11.

In SUSY events, the presence of two SFOS leptons can also be due to processes different from $\tilde{\chi}_2^0 \rightarrow \tilde{l}_R l \rightarrow \tilde{\chi}_1^0 l^+ l^-$ decay. If the two leptons are independent of each other, one would expect equal amounts of SFOS leptons and different flavour opposite sign (DFOS) leptons. Their distributions should also be identical. The background SFOS contribution can hence be removed by subtracting the DFOS events. Figure 12 shows the same SFOS distribution for SUSY events together with the distribution of the DFOS lepton pairs. The flavour subtracted SFOS dilepton pair distributions for both SUSY and $t\bar{t}$ background are shown in Figure 13 for an integrated luminosity of 1 fb^{-1}. The $t\bar{t}$ background contribution after the flavour subtraction is close to zero since the lepton pairs are always uncorrelated. The Z+jets, instead, remains unchanged after the flavour subtraction, since the two selected leptons come from the Z.

The numbers of SUSY and background dilepton pairs surviving cuts are respectively 913 and 224, giving a signal to background ratio of 4.1. A statistical significance of 5 sigma, calculated using S_{cP} [14], can be obtained with 14 pb^{-1} of integrated luminosity.

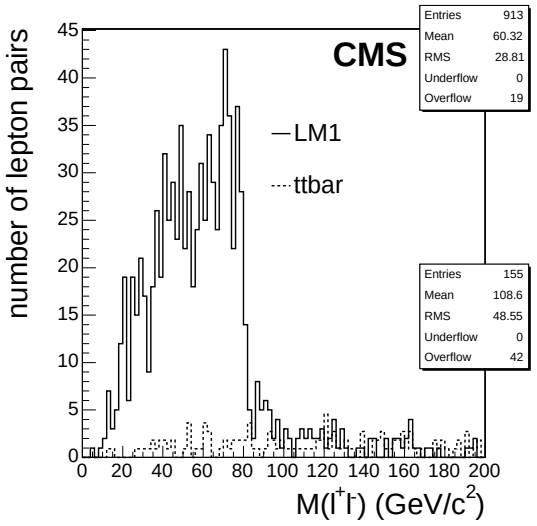

Figure 11: Same flavour opposite sign lepton pair distributions of SUSY and $t\bar{t}$ events for 1 fb^{-1}.

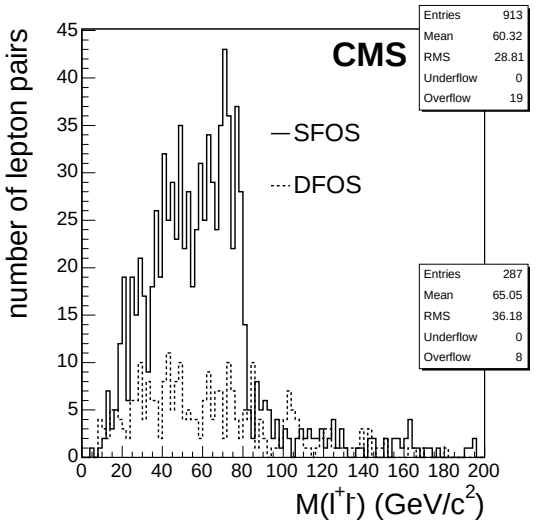

Figure 12: SFOS and DFOS distributions of events for 1 fb^{-1}.

The value of the end point can be extracted by fitting the flavour subtracted distribution with a convolution of a triangle and a Gaussian function (Fig. 14). The width of the smearing is left as a free parameter of the fit, although, in a real analysis, a constraint can be obtained from the experimental resolution in the dilepton invariant mass reconstructed in well known channels, such as Z$\rightarrow$ ee and Z$\rightarrow$ $\mu\mu$. The value obtained from the fit is:

$$M_{ll}^{max} = 80.42 \pm 0.48\,\mathrm{GeV}/c^2 \tag{1}$$

where the error quoted is only statistical. The theoretical end point value is 81.04 GeV/c^2.

The SFOS and DFOS distributions of SUSY events for an integrated luminosity of 9.2 fb^{-1} are shown in Figure 15. The result of the fit is shown superimposed over the flavour subtracted distribution in Figure 16. The measured end point is

$$M_{ll}^{max} = 80.56 \pm 0.17\,\mathrm{GeV}/c^2 \tag{2}$$

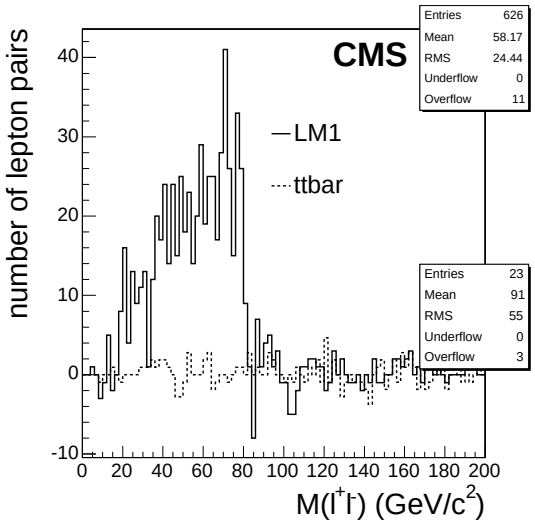

Figure 13: Flavour subtracted distributions of SUSY and $t\bar{t}$ events for 1 fb^{-1}.

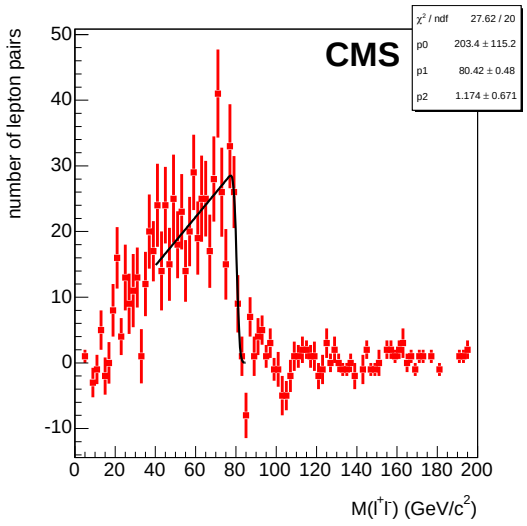

Figure 14: Flavour subtracted distributions of SUSY and $t\bar{t}$ events for 1 fb^{-1}. The fit function is shown superimposed.

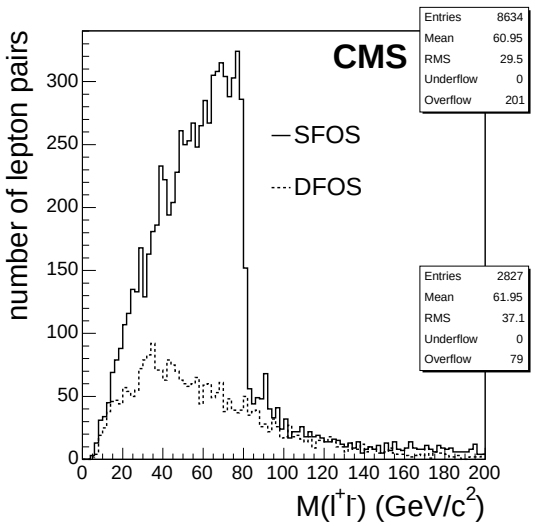

Figure 15: SFOS and DFOS distributions of SUSY events for 9.2 fb^{-1}.

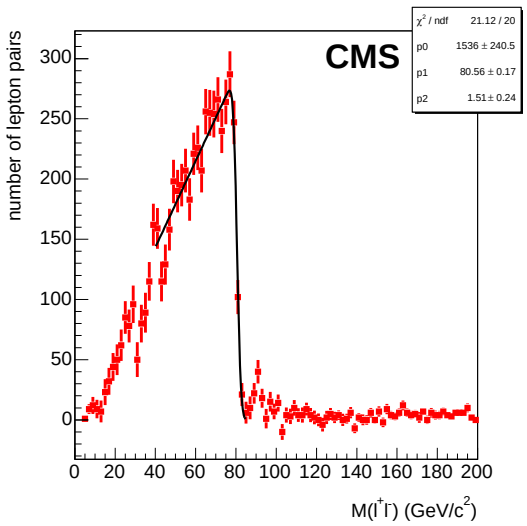

Figure 16: Flavour subtracted distributions of SUSY and $t\bar{t}$ events for 9.2 fb^{-1}. The fit function is shown superimposed.

5 Systematics

5.1 Misalignment

The effect of tracker and muon chambers misalignment on endpoint has been studied in two scenarios [15]:

- FirstData, simulating the misalignment during the first 6 months of data taking, roughly up to 1 fb^{-1} of integrated luminosity;
- LongTerm, simulating the residual misalignment after a longer running time, from 1 to 10 fb^{-1} of integrated luminosity.

Either the effects on endpoint position and on selection efficiency have been studied. For both cases, all selection cuts have been applied to signal events.

For the FirstData scenario, selection efficiencies are lowered by $\sim 30\%$ for muons and by $\sim 10\%$ for electrons. Taking into account separately the effects of tracker and muon system on muons shows that the loss of efficiency is almost exclusively due to the tracker misalignment. Even in this scenario, the endpoint in the invariant mass distributions is still visible (Fig. 17, 18).

In the LongTerm scenario, effects are obviously less evident, with respect to the FirstData scenario: the efficiencies are lowered by $\sim 13\%$ for muons and $\sim 2\%$ for electrons. Invariant mass distributions are marginally affected, and the endpoint is clearly visible (Fig. 19, 20).

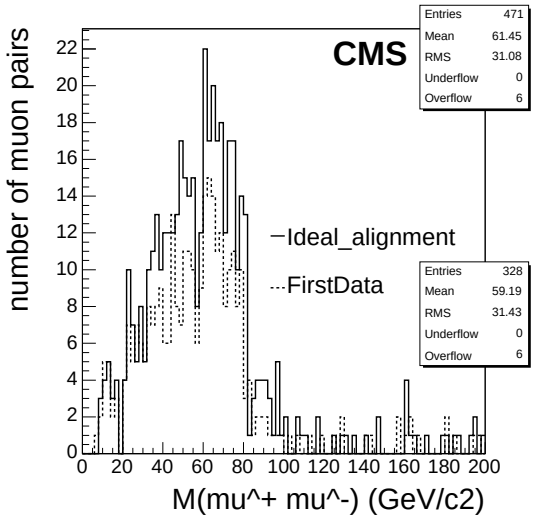

Figure 17: Muon invariant mass distribution for ideal alignment and in first data scenario.

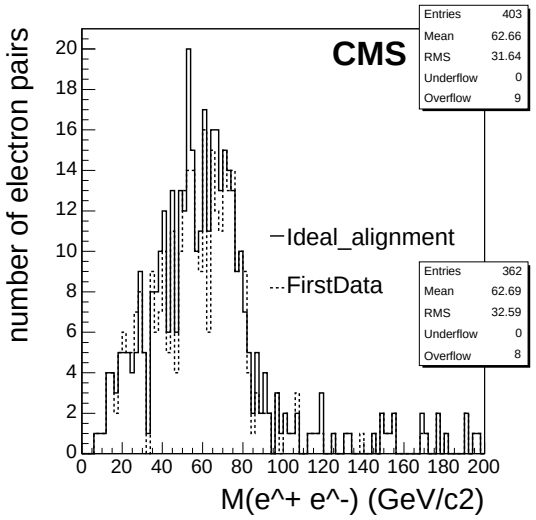

Figure 18: Electron invariant mass distribution for ideal alignment and in first data scenario.

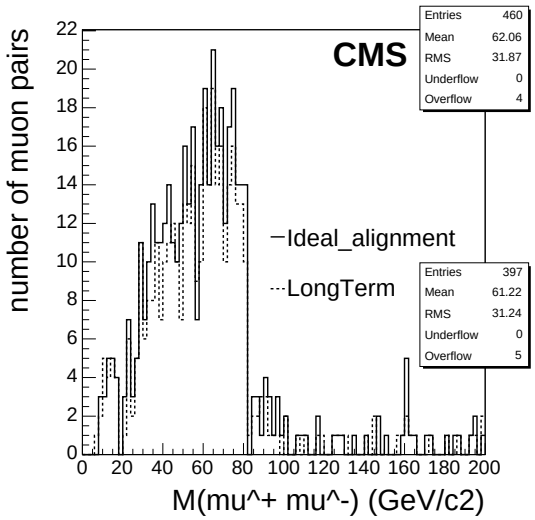

Figure 19: Muon invariant mass distribution for ideal alignment and in long term scenario.

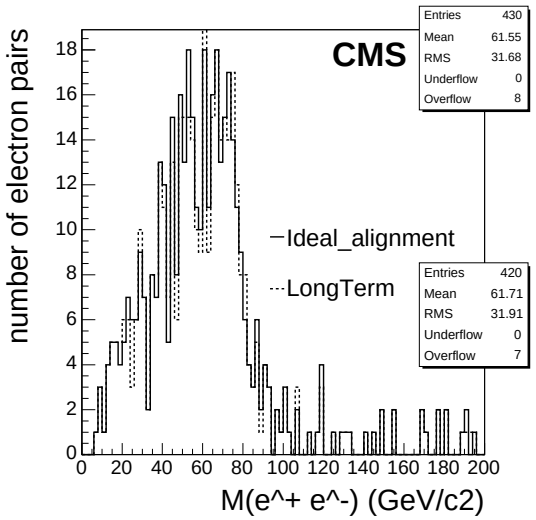

Figure 20: Electron invariant mass distribution for ideal alignment and in long term scenario.

The final selection efficiencies for SUSY events at LM1 point are 1.2% for first data misalignment (1.5% for long term), corresponding to an expectation of 641 (762) events surviving cuts for 1 fb^{-1} of integrated luminosity (Tab.

Table 7: Final selection efficiencies at LM1 for ideal alignment and the two scenarios considered, and the relative number of events passing cuts for 1 fb^{-1} of integrated luminosity.

	ε_{MEAS}	N. ev. in 1 fb^{-1}
Ideal alignment	0.016	853
First data	0.012	641
Long term	0.015	762

Table 8: Effect of JES systematic uncertainty on signal at LM1 and $\mathrm{t\bar{t}}$ background for 1 fb^{-1} of integrated luminosity, with and without taking into account propagation of errors to MET. The relative fractional change of the number of events is shown.

	JES	
	-0.07	+0.07
LM1 (No MET propagation)	-0.005	0.011
LM1 (MET propagation)	-0.079	0.079
$\mathrm{t\bar{t}}$ (No MET propagation)	-0.044	0.01
$\mathrm{t\bar{t}}$ (MET propagation)	-0.135	0.198

7). For reference, without misalignment an efficiency of 1.6% is expected, corresponding to 853 events in 1 fb^{-1}.

The position of the endpoint is also slightly affected by misalignment. The shift, estimated through fits similar to the ones described in the previous sections, is of about 1 GeV/c^2 in the FirstData scenario.

5.2 Jet and electron energy scale

The error due to the absolute electron energy scale (ElecES) and jet energy scale (JES) uncertainties has also been evaluated. An uncertainty of 0.25% at all integrated luminosities has been considered for the ElecES [16], while 7% for 1 fb^{-1} and of 2% for ≥ 10 fb^{-1} are the values used as JES uncertainty.

For $\mathrm{t\bar{t}}$ background, at 1 fb^{-1}, a variation in the number of expected events of $-4\% \div +1\%$ is expected without propagation of errors to MET, and of $-14\% \div +20\%$ if propagation to MET is taken into account. For signal at LM1, at 1 fb^{-1}, contribution of JES on the number of events passing cuts is $\sim 0.5 \div 1.\%$ without propagation to MET, and 8% propagating errors to MET (Tab. 8).

At ≥ 10 fb^{-1}, the JES uncertainty gives a variation of $-9\% \div +5\%$ in the number of expected background events taking into account the propagation to MET. The effect in the number of signal events is 0.4% (2%) without (with) propagation of errors to MET (Tab. 9).

Effect of ElecES uncertainty is much less pronounced, being less than 1% for $\mathrm{t\bar{t}}$ background and a fairly negligible $\sim 0.1\%$ for LM1, at all integrated luminosities.

The integrated luminosity needed to reach 5 sigma significance at LM1, when a 20% systematic error is taken into account for the background, is of 17 pb^{-1}. This figure has been calculated using S_{cP}. In this case we also checked the result using Z_{Bi} [17, 18], which gives a fairly similar value, 19 pb^{-1}.

The effect of the energy scale uncertainties on the determination of the dilepton edge were evaluated using the full sample corresponding to 9.2 fb^{-1}, in order to minimise as much as possible the statistical error. The position of the endpoint is shifted by about ± 0.15 GeV/c^2 by a mismeasurement of ElecES, while the JES uncertainty gives a negligible shift (Tab. 10).

5.3 Other sources

Other possible sources of systematic uncertainties are the scale uncertainty on NLO cross section, PDF uncertainty and luminosity error. For the main background, inclusive $\mathrm{t\bar{t}}$, these errors are taken to be respectively 2.5% [19], 5%, and 5% [20].

Table 9: Effect of JES systematic uncertainty on signal at LM1 and $t\bar{t}$ background for 10 fb^{-1} of integrated luminosity, with and without taking into account propagation of errors to MET. The relative fractional change of the number of events is shown.

	JES	
	-0.07	+0.07
LM1 (No MET propagation)	-0.004	0.004
LM1 (MET propagation)	-0.023	0.023
$t\bar{t}$ (No MET propagation)	-0.01	< 0.01
$t\bar{t}$ (MET propagation)	-0.073	0.044

Table 10: Effect of JES and ElecES systematic errors on the position of the dilepton edge. The relative fractional change of the number of events is shown.

		ElecES		
		-0.01	0.00	+0.01
JES	-0.07	80.38±0.18	80.53±0.17	80.63±0.17
	0.00	80.42±0.17	80.56±0.17	80.68±0.17
	+0.07	80.40±0.20	80.54±0.17	80.66±0.17

6 Scan

In order to check the observability of SUSY events in the leptons+jets+missing transverse energy final state, a scan of the mSUGRA plane $(m_0,\, m_{1/2})$ has been performed. Keeping $A_0 = 0$, $\mathrm{sign}\,(\mu) = +$, and $\tan(\beta) = 10$, the $(m_0,\, m_{1/2})$ plane has been scanned starting from $m_0\ (m_{1/2}) = 100$ GeV/c^2 and using a step of 50 GeV/c^2 for $m_0\ (m_{1/2}) \leq 600$ GeV/c^2 and a step of 100 GeV/c^2 for 700 GeV/c^2 $< m_0\ (m_{1/2}) \leq 1000$ GeV/c^2. The number of events produced at each point ranges from 10k to 100k, increasing with decreasing $m_{1/2}$. Events have been generated with PYTHIA 6.225 interfaced with ISAJET 7.69 and then passed to FAMOS 1.4.0 [21], the software for the fast simulation of the CMS detector. A pileup of 3.5 events per bunch crossing, corresponding to the low luminosity case ($2 \cdot 10^{33}$ cm^{-2}s^{-1}) was considered. Background used is the same as in the analysis at LM1 point. The same selection cuts for background and signal have been used. The HLT was simulated applying cuts to the offline objects.

The visibility of signal over background has been looked for in the unsubtracted dilepton histogram. Using the number S of signal events and B of background events surviving cuts, significance has been calculated with S_{cP}.

When systematic uncertainties are taken into account for scan, the hypothesis done on the signal is tested against the background modified by the systematic error. Obviously, only those uncertainties increasing the number of expected background events are of interest. The uncertainty taken into account in the number of background events is 20% at 1 fb^{-1} , and 5% at 10 and 30 fb^{-1} , coming mainly from JES.

6.1 Results

Results of the scan are shown for 1, 10, and 30 fb^{-1} of integrated luminosity. If systematic uncertainties are not taken into account, with 1 fb^{-1} of integrated luminosity, 5σ statistical significance can be reached up to $m_{1/2} \sim 350$ GeV/c^2 for all the m_0 considered values, while with 30 fb^{-1} the signal is observable up to $m_{1/2} \sim 700$ GeV/c^2 for $m_0 < 200$ GeV/c^2 and up to $m_{1/2} \sim 550$ GeV/c^2 for the remaining m_0 values (Fig. 21). With systematic uncertainties, the range is reduced to $m_{12} < 300$ GeV/$c^2$for 1 fb^{-1}of integrated luminosity, and $m_{12} < 400$ GeV/c^2 for 30 fb^{-1}.

7 Conclusions

The observability of the $\tilde{\chi}_2^0 \rightarrow \tilde{l}_R l \rightarrow \tilde{\chi}_1^0 l^+ l^-$ decay produced in SUSY chains through the two same flavour opposite sign lepton pairs + Jets + Missing Transverse Energy final state has been studied at mSUGRA benchmark point LM1 ($\mathrm{m}_0 = 60$ GeV/c^2, $\mathrm{m}_{1/2} = 250$ GeV/c^2, $\mathrm{A}_0 = 0$, $\tan\beta = 10$, $\mathrm{sgn}(\mu) = +1$). The end point in the dilepton invariant mass distribution can be measured with a statistical error of ~ 0.5 GeV/c^2 at 1 fb^{-1} and ~ 0.15 GeV/c^2 at 9.2 fb^{-1}. The main systematic uncertainties have also been evaluated: the misalignment of the

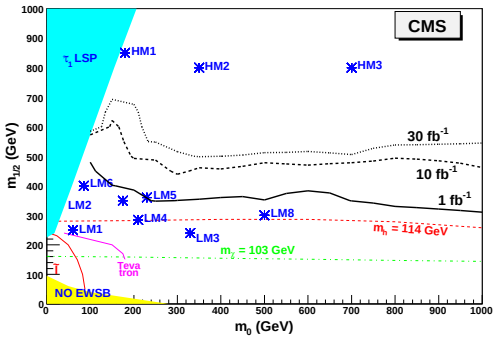

Figure 21: Discovery reach at tanβ = 10 for an integrated luminosity of 1, 10, and 30 fb^{-1}, when no systematic uncertainties are taken into account.

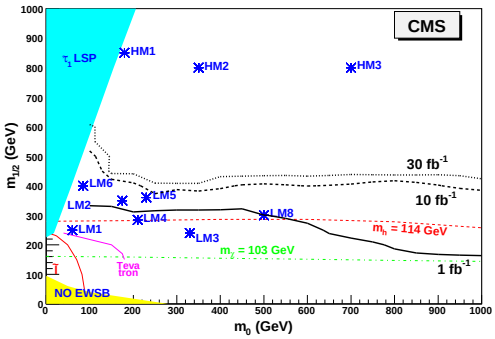

Figure 22: Discovery reach at tanβ = 10 for an integrated luminosity of 1, 10, and 30 fb^{-1}, when systematic uncertainties are taken into account.

CMS Tracker can affect the signal, decreasing the efficiency of about 21% in the first months of data taking and of about 9% in a longer period, when a better alignment of the Tracker can be obtained from data. The systematic uncertainty on the end point measurement due to the misalignment of the Tracker is of about 1 GeV/c^2. The effect of the muon misalignment has been demonstrated to be negligible. The systematic uncertainty due to the jet and electron energy scale uncertainty is 8% on the number of selected signal events for 1 fb^{-1} of integrated luminosity and 2% for 9.2 fb^{-1}. The effect of the energy scales in the end point measurement is of 0.15 GeV/c^2. The effect of the systematic uncertainty on the main backgrounds has also been evaluated. The effect of the energy scale in the $\mathrm{t\bar{t}}$ is a 20% increase of the number of selected events.

The signal to background ratio at LM1, after all the selection cuts, is 4.1. The integrated luminosity needed to reach 5 sigma significance is 14 pb^{-1} (S_{cP}) without systematics, and 17 pb^{-1} (S_{cP}) or 19 pb^{-1} (Z_{Bi}) with systematic uncertainties taken into account.

The value of the end point measurement is:

$$M_{ll}^{max} = 80.42 \pm 0.48(\mathrm{stat}) \pm 1(\mathrm{misal.}) \pm 0.15(\mathrm{ElecES})\ \mathrm{GeV}/c^2 \text{ for } 1\ \mathrm{fb}^{-1} \quad (3)$$

$$M_{ll}^{max} = 80.56 \pm 0.17(\mathrm{stat}) \pm 0.5(\mathrm{misal.}) \pm 0.15(\mathrm{ElecES})\ \mathrm{GeV}/c^2 \text{ for } 9.2\ \mathrm{fb}^{-1} \quad (4)$$

The observability of the SUSY events in the leptons + jets + missing transverse energy final state in the m_0, $m_{1/2}$ plane has also been evaluated in the unsubtracted case. Without systematic uncertainties on background, the 5 σ discovery reach goes, for a large range of m_0 values, from $m_{12} < 350$ GeV/c^2 at 1 fb^{-1} to $m_{12} < 550$ GeV/c^2 at 30 fb^{-1}. When systematic uncertainties are taken into account, the reach is reduced, and ranges from $m_{12} < 300$ GeV/c^2 (1 fb^{-1}) to $m_{12} < 400$ GeV/c^2 (30 fb^{-1}).

8 Acknowledgments

We would like to thank L. Pape and M. Spiropulu for their precious guidance, C. Delaere for trigger questions, S. Bityukov for his help with significance calculation. Many thanks also to Darin Acosta and Bob Cousins for having read the manuscript and having given precious suggestions.

References

[1] B. C. Allanach, C. G. Lester, M. A. Parker and B. R. Webber, JHEP **0009** (2000) 004 [arXiv:hep-ph/0007009]

[2] M. Battaglia *et al.* [arXiv:hep-ph/0306219]

[3] W.Beenakker, R.Hoepker, M.Spira, "PROSPINO: A Program for the Production of Supersymmetric Particles in Next-to-leading Order QCD" [arXiv:hep-ph/9611232]

[4] T. Sjöstrand, P. Edén, C. Friberg, L. Lönnblad, G. Miu, S. Mrenna and E. Norrbin, Computer Phys. Commun. 135 (2001) 238 [LU TP 00-30, arXiv:hep-ph/0010017]

[5] http://www.phy.bnl.gov/∼isajet/

[6] CMS Coll, Object oriented Simulation for CMS Analysis and Reconstruction, http://cmsdoc.cern.ch/oscar/

[7] CMS Coll., Object oriented Reconstruction for CMS Analysis, http://cmsdoc.cern.ch/orca/

[8] http://cmsdoc.cern.ch/cms/production/www/html/general/index.html

[9] S. Baffioni *et al.*, **CMS NOTE-2006/040**

[10] A. Pukhov *et al.* [arXiv:hep-ph/9908288]

[11] V. Konoplianikov *et al.*, **CMS NOTE-2006/042**

[12] CMS Coll., CMS Physics TDR, Volume 1, **CERN-LHCC-2006-001**

[13] J .Done *et al.*, CDF/ANAL/EXOTIC CDFR/4909

[14] S. I. Bityukov, N. V. Krasnikov, "On observability of signal over background", **NIM A** 452: 518-524, 2000

[15] I. Belotelov *et al.*, **CMS NOTE-2006/008**

[16] V. Büge *et al.*, **CMS NOTE-2006/061**

[17] J. T. Linneman [arXiv:physics/0312059]

[18] K. Cranmer [arXiv:physics/0511028]

[19] D. Chakraborty, J. Konigsberg, D. Rainwater [arXiv:hep-ph/0303092]

[20] M. Baarmand, M. Hashemi, A. Nikitenko, **CMS NOTE-2006/056**

[21] CMS Coll., http://cmsdoc.cern.ch/famos/